Available online at www.sciencedirect.com
ScienceDirect
Trans. Nonferrous Met. Soc. China 32(2022) 4113−4128

Transactions of
Nonferrous Metals
Society of China
www.tnmsc.cn

Thermodynamic modeling of antimony removal from complex resources in copper smelting process

Song-song WANG[1,2], Qin-meng WANG[1,2], Xue-yi GUO[1,2],
Qing-hua TIAN[1,2], Sheng-li QU[3], Zhi WANG[4], Ming-xing HUANG[1,2]

1. School of Metallurgy and Environment, Central South University, Changsha 410083, China;
2. National & Regional Joint Engineering Research Center of Nonferrous Metal Resources Recycling, Changsha 410083, China;
3. Shandong Humon Smelting Co., Ltd., Yantai 264109, China;
4. Dongying Fangyuan Nonferrous Metals Co., Ltd., Dongying 257091, China

Received 26 September 2021; accepted 24 January 2022

Abstract: This work investigated the reaction mechanism of Sb in copper smelting process. The difference of multi-phase distribution of Sb in four typical copper smelting processes was analyzed. A multi-phase equilibrium model of the oxygen-enriched bottom-blow copper smelting process was developed. The impacts of Cu, S, and Sb concentrations in raw materials on Sb distribution in multiphases were researched. This model was also used to investigate the effect of process factors such as copper matte grade, oxygen-enriched concentration, smelting temperature, and oxygen/ore ratio (ratio of oxygen flow rate under standard conditions to concentrate charge rate) on Sb distribution behavior. The results showed that calculation data were in good agreement with the actual production results and literature data. Increasing the Cu content and decreasing the S and Sb contents in the concentrate, increasing the copper matte grade, oxygen/enriched concentration, and oxygen-ore ratio, and at the same time appropriately reducing the smelting temperature are conducive to the targeted enrichment of Sb into the slag. Modeling results can provide theoretical guidance for the clean and efficient treatment of complex resources and the comprehensive recycling of associated elements.

Key words: copper; oxygen-enriched smelting; Sb; reaction mechanism; distribution behavior

---

1 Introduction

With the depletion of high-quality resources, polymetallic associated resources and urban minerals are becoming critical raw materials for copper smelting [1]. These resources contain not only valuable metals (e.g., copper, gold, silver, and platinum), but also hazardous elements (e.g., lead, antimony, bismuth, and arsenic) [2]. How to efficiently recover valuable metals while avoiding environmental pollution by harmful elements [3−6] is a current research hotspot.

The previous studies [7,8] have focused on recovering valuable metals from complex resources synergistic treatment in the copper smelting process. Hazardous elements are removed by volatilization or slagging [9−11] to avoid the impact on copper matte or copper products. However, less attention has been paid to the efficient separation of accompanying elements. Due to the chemical similarity of arsenic and antimony [12,13], there are difficulties in separating them from dust outside the furnace by physical and chemical methods [14,15]. Therefore, the reaction mechanism and multi-phase distribution behavior of antimony in the smelting process need to be investigated to dissolve antimony in the slag while arsenic volatilizes into

---

Corresponding author: Qin-meng WANG, Tel: +86-731-88876255, E-mail: qmwang@csu.edu.cn

DOI: 10.1016/S1003-6326(22)66082-5

the gas phase [16,17]. Arsenic and antimony are separated during the copper smelting, laying the foundation for the subsequent recovery of arsenic from dust and antimony from slag, respectively.

Many researchers have studied the multi-phase distribution behavior of antimony in copper smelting. The fundamental thermodynamic data of Sb in copper matte and slag are measured [18−23]. The distribution ratio of Sb in the copper matte−slag equilibrium system is calculated [24−26]. Most of the above studies are carried out at constant temperature/pressure/spinel-saturated/silica-saturated systems in the laboratory. The experimental results could guide theoretical studies of phase equilibrium but have limited significance for practical production guidance. MITEVSKA and ŽIVKOVIĆ [27], PADILLA and RUIZ [28] and TASKINEN et al [29] calculated the distribution ratio of Sb in the actual production process. CHAUBAL et al [30], FONT and REDDY [31], SURAPUNT [32] and CHEN et al [22] established a thermodynamic model for copper smelting and studied the distribution behavior of the associated element Sb. The distribution difference of Sb among different processes is attributed to the copper matte grade. However, the reaction process and distribution regulation of Sb in different copper smelting processes were less studied.

In this study, the reaction mechanism of Sb in the copper smelting process was obtained, and factors affecting the distribution of elements in different smelting processes were revealed. A multi-phase equilibrium thermodynamic model of Sb was developed by combining actual production industrial data, which was used to model the distribution of Sb among phases under varied operating conditions. The raw material compositions and process parameters were optimized to achieve the enrichment of Sb into the slag, which reduces the impact on the extraction of arsenic from dust and the hazard to the smelting environment, and at the same time provides the high-quality raw material for the comprehensive recovery of Sb from slag [33].

2 Reaction mechanism

2.1 Reaction thermodynamics

To improve the high-temperature processes for removing impurity elements, basic knowledge about the impurity element reaction mechanism and distribution is necessary. The most likely reactions of Sb in copper smelting processes can be concluded as follows.

Sb is one of the major deleterious impurities in copper sulfide concentrates, where the element occurs mainly as sulfide minerals. Common mineral of Sb is tetrahedrite ($Cu_{12}Sb_4S_{13}$) [28,34]. At a typical copper smelting temperature, the decomposition reaction of $Cu_{12}Sb_4S_{13}$ easily takes place according to Reaction (1):

$$2Cu_{12}Sb_4S_{13}(s) \rightarrow 12Cu_2S(l)+4Sb_2S_3(l)+S_2(g) \quad (1)$$

Due to high temperature and the prevailing oxygen pressure, these sulfide compounds can be oxidized [35,36] as follows:

$$Sb_2S_3(l)=Sb_2S_3(g) \quad (2)$$

$$Sb_2S_3(l)+O_2(g)=2SbS(g)+SO_2(g) \quad (3)$$

$$1/3Sb_2S_3(g)+O_2(g)=1/3Sb_2(g)+SO_2(g) \quad (4)$$

$$2/3SbS(g)+O_2(g)=2/3SbO(g)+2/3SO_2(g) \quad (5)$$

$$Sb_2(g)+O_2(g)=2SbO(g) \quad (6)$$

$$4SbO(g)+O_2(g)=2Sb_2O_3(l) \quad (7)$$

Unreacted sulfides in the concentrate react with oxygen or oxides in the slag phase.

$$1/3Sb_2S_3(l)+O_2(g)=1/3Sb_2(g)+SO_2(g) \quad (8)$$

$$1/3Sb_2S_3(l)+O_2(g)=2/3Sb(l)+SO_2(g) \quad (9)$$

$$1/2Sb_2S_3(l)+Sb_2O_3(l)=3Sb(l)+3/2SO_2(g) \quad (10)$$

$$Sb_2O_3(l)+9FeO(l)=2Sb(l)+3Fe_3O_4(l) \quad (11)$$

With enough oxygen present, Sb reacts with gaseous oxygen as follows:

$$4/3Sb(l)+O_2(g)=2/3Sb_2O_3(l) \quad (12)$$

To control the slaggy properties and reduce the Cu and Fe_3O_4 contents in the slag, reducing agents are charged into the furnace. The oxides of Sb are reduced as follows:

$$Sb_2O_3(l)+3/2C(s)=Sb_2(g)+3/2CO(g) \quad (13)$$

$$Sb_2O_3(l)+3CO(g)=Sb_2(g)+3CO_2(g) \quad (14)$$

$$Sb_2O_3(l)+3C(s)=2Sb(l)+3CO(g) \quad (15)$$

$$Sb_2O_3(l)+3CO(g)=2Sb(l)+3CO_2(g) \quad (16)$$

$$3Fe_3O_4(l)+3/2C(s)=9FeO(l)+3/2CO_2(g) \quad (17)$$

$$Fe_3O_4(l)+CO(g)=3FeO(l)+CO_2(g) \qquad (18)$$

The Gibbs energy change data of the above reactions are calculated and plotted in Fig. 1.

As shown in Fig. 1(a), the reactions can proceed spontaneously at copper smelting temperature. The Gibbs energy change of oxidation reaction in copper matte is higher than that in other phases, which seems to indicate that Sb is preferentially distributed in the copper matte during the smelting process. Figure 1(b) shows that Sb_2O_3 is preferentially reduced compared to Fe_3O_4 in the presence of reducing agents. The migration evolution of Sb during copper smelting is shown in Fig. 2.

In the furnace, the $Cu_{12}Sb_4S_{13}$ preferentially decomposes into simple sulfides (Cu_2S, CuS, Sb_2S_3, and S_2) during the falling of the concentrates. The sulphide of Sb is oxidized to SbS(g), SbO(g), and Sb_2O_3(l). SbS(g) and SbO(g) are removed to the gas phase, and Sb_2O_3(l) falls into the melting bath. In slag, there are interactions among Sb_2S_3(l), gaseous oxygen and oxides. Sb(l) transports into copper matte, Sb_2O_3(l) remains in slag and Sb_2(g) vaporizes into gas and then is oxidized. Sb(l) in the copper matte phase reacts with oxygen. The oxidation product Sb_2O_3(l) migrates into the slag phase. The bubbles carrying SbO(g) are oxidized as they pass through the slag layer from copper matte. Under certain smelting conditions, the above reactions reach equilibrium, and the distribution ratio of Sb among copper matte, slag, and flue gas can be obtained. In practice, Sb can be enriched in a phase by enhanced reactions.

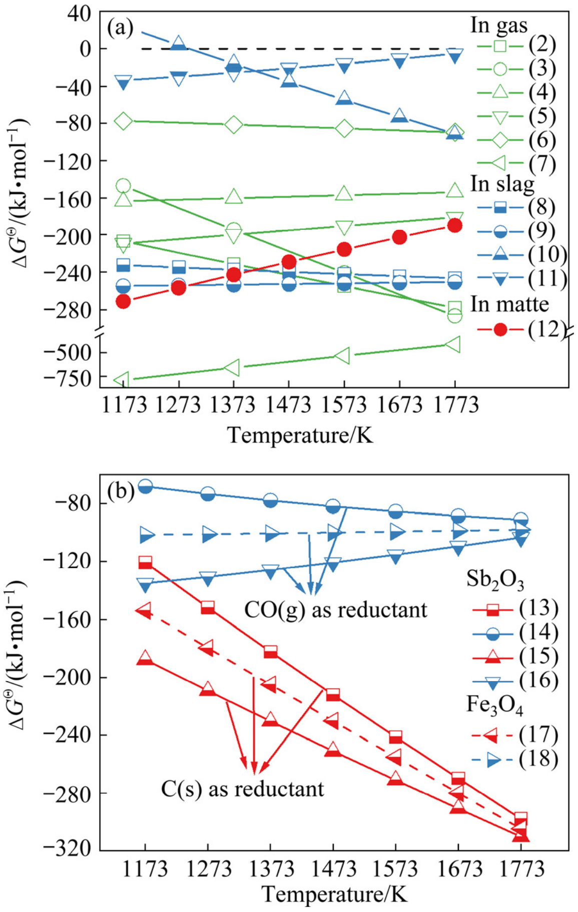

Fig. 1 Reaction Gibbs free energy change of Sb-bearing species without (a) and with (b) reductant

2.2 Difference of Sb distribution

Modern enhanced copper smelting processes include flash smelting (FS) technology [29], oxygen-enriched bottom-blowing smelting (OBBS) technology, oxygen-enriched side-blow smelting

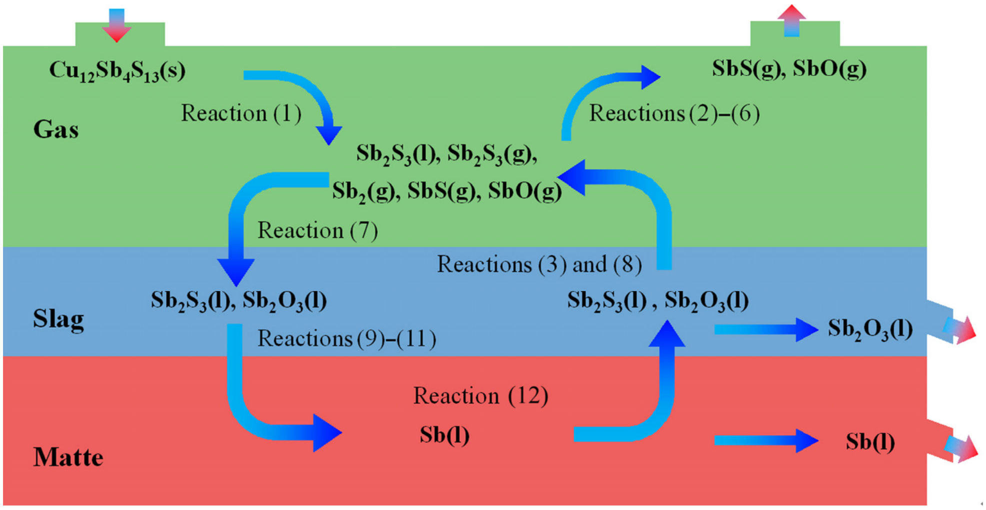

Fig. 2 Schematic diagram of Sb reaction mechanism and distribution

(OSBS) technology [37,38] and oxygen-enriched top-blow smelting (OTBS) technology [39,40]. The position of oxygen-enriched blowing, charge method, and process parameters (copper matte grade, temperature, slag type, and reducing agent) are different in various copper smelting processes. Therefore, the reaction process of Sb is quite diverse, which results in different multi-phase distributions of Sb. The distribution of Sb and technological properties in the typical copper smelting process are listed in Table 1.

Table 1 shows that most Sb stays in copper matte in FS [41], transfers into slag in OBBS, and volatilizes into gas in OSBS [42] and OTBS [43]. In flash smelting reaction shaft where oxygen-enriched air and concentrates are sprayed together, Reaction (7) is the primary reaction. Then, Reactions (10) and (11) occur, and the product of Sb falls into copper matte. Reaction (12) proceeds slowly for the lack of sufficient oxygen in copper matte [44]. In the bath smelting process, oxygen-enriched gas is blown in the slag or copper matte. The oxygen partial pressure and temperature in the gas phase are lower compared with FS. Thus, the distribution rates of Sb in the gas are high. With sufficient oxygen, Sb in the copper matte is oxidized and transferred into the slag in OBBS. But for OSBS and OTBS, Reactions (13) and (14) proceed with reducing agents, and most Sb is continuously vaporized into the gas phase. Smelting temperature and oxygen-enriched concentration are essential important factors affecting the multi-phase distribution of Sb [26]. The high melting temperature and low oxygen-enriched concentration favor the volatilization of Sb into the gas phase.

The above analysis shows that the removal rate of Sb is low in FS technology, and Sb and As volatilize into the flue gas at the same time in OSBS and OTBS, which affects the purification of As. For OBBS, As is volatilized into the gas phase while Sb is transferred in slag, achieving enhanced separation of the impurity elements. The OBBS has apparent advantages in complex resources synergistic treatment in the copper smelting process.

3 Model development

A thermodynamic model of Sb in OBBS is established when the complex primary and secondary resources are co-processed. The raw material compositions and process parameters are optimized. The directional distribution regulation of hazardous elements is achieved. Sb is enriched into slag. The removal rate of Sb is high, while the impact of Sb on As-bearing compound purification from dust is avoided.

3.1 Thermodynamic model

The total Gibbs free energy is used to measure how close the system is to the equilibrium state, which can be calculated by Eq. (19) [45]:

$$G(n,T,P)=\sum_{j=1}^{N_\mathrm{P}}\sum_{i=1}^{N_\mathrm{C}}n_{ij}u_{ij}=\sum_{j=1}^{N_\mathrm{P}}\sum_{i=1}^{N_\mathrm{C}}n_{ij}\left[\Delta G_{ij}^{\Theta}+RT\ln\left(\gamma_{ij}\cdot n_{ij}\Big/\sum_{k=1}^{N_\mathrm{C}}n_{kj}\right)\right] \tag{19}$$

where n, T and P are the mole number of component, thermodynamic temperature and pressure, respectively, N_P and N_C are the numbers of phases and component in phases, respectively. ΔG_{ij}^{Θ} is the standard Gibbs free energy change of component i in phase j, R is the molar gas constant, γ_{ij} is the activity coefficient of component i in phase j, n_{ij} is the mole number of component i in phase j, and u_{ij} is the chemical potential of component i in phase j.

The minimum Gibbs free energy principle is used to develop a multi-phase equilibrium model of Sb in copper smelting, because it is difficult to carry out experimental research directly on the actual production scale. The model is solved, and the distribution of elements is obtained when the system achieves thermodynamic equilibrium.

Table 1 Distribution of Sb and technological properties in different processes

Technology	Sb distribution/%			Oxygen-enriched concentration/%	Smelting temperature/K	Oxygen blowing position
	Matte	Slag	Gas			
FS	59.32	35.28	5.40	70−80	1523−1623	In gas
OBBS	12.48	71.15	16.37	70−78	1453−1543	In matte
OTBS	31.00	3.00	66.00	50−60	1453−1523	In slag
OSBS	15.00	29.00	57.00	35−50	1473−1573	In slag

3.2 Thermodynamic data

The Gibbs free energy change data and the activity coefficient of compounds are critical thermodynamic parameters for the model. To simplify the actual production process, some assumptions are made in this work. The dissolution form of antimony is atomic form Sb in copper matte [46] and mono-nuclear atom base oxide $SbO_{1.5}$ in slag [47], respectively. It was reported that monoanion form of oxides shows a constant activity coefficient over an extensive range of composition [48,49]. SbO and SbS are the predominant forms present in the gas phase. The selected thermodynamic data for Sb species are listed in Table 2.

Table 2 Selected Gibbs free energy change for Sb species

Reaction	ΔG^{Θ}_{ij}/(J·mol^{-1})	Source
$0.5Sb_2(g)=Sb(l)$	−86942.50+46.93T	[50]
$0.5Sb_2(g)+0.5O_2(g)=SbO(g)$	58618.10−9.93T	[51]
$0.5Sb_2(g)+0.5S_2(g)=SbS(g)$	44162.60−18.06T	[51]
$Sb(l)+0.75O_2(g)=SbO_{1.5}(l)$	−334820+114.23T	[48]

The activity coefficient of Sb (γ'_{Sb}) in copper matte can be described by Eq. (20):

$$\gamma_{Sb}=-0.1423+0.3457G_m-0.18G_m\cdot\lg G_m \tag{20}$$

where G_m is the copper matte grade.

The γ_{Sb} decreases with an increasing matte grade, which implies that increasing copper matte grade is not conducive to antimony removal. The activity of Sb in Cu−Fe−S−Sb system is plotted against the antimony concentration in Fig. 3 compared with MENDOZA et al [19] and CHEN et al [22]. The Sb activity shows negative deviation from ideality and is increased with increasing Sb content in copper matte. In the present work (PW), the activity is slightly reduced due to the reduction of Fe concentration. However, the activity data show good consistency with previous studies at T=1501 K and molar fraction of Fe x_{Fe}=0.12. It is evident that the model can represent the behavior of Sb in such copper matte.

The activity coefficient of $SbO_{1.5}$ in FeO_x−SiO_2 slag can be represented as Eq. (21) and plotted in Fig. 4.

$$\gamma_{SbO_{1.5}}=\exp(1055.66/T) \tag{21}$$

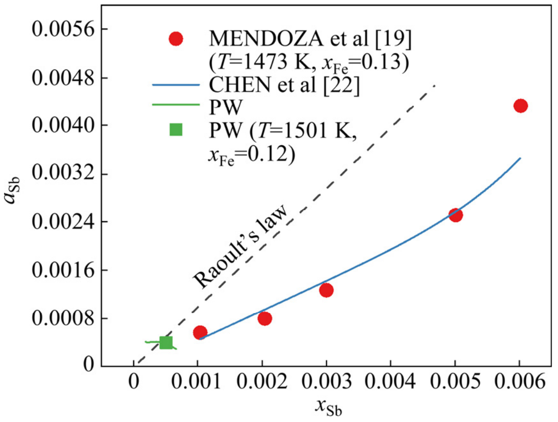

Fig. 3 Sb activity (a_{Sb}) in Cu−Fe−S−Sb ternary system

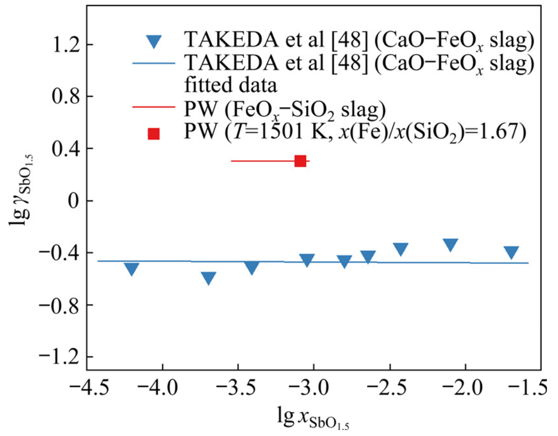

Fig. 4 $SbO_{1.5}$ activity coefficient in iron silicate slag and calcium ferrite slag

TAKEDA et al [48] measured the activity coefficient of $SbO_{1.5}$ in FeO_x−CaO slags, which is independent of $SbO_{1.5}$ concentration as mentioned above. In present work, FeO_x−SiO_2 slag is adopted in OBBS, in which the activity coefficient is higher than that of FeO_x−CaO slags. Sb oxide is acidic, which tends to form an oxide with basic flux. The activity coefficient of $SbO_{1.5}$ decreases with the increase of CaO, which indicates a higher distribution of Sb in FeO_x−CaO slag [23,51,52].

3.3 Model validation

3.3.1 Basic conditions

Table 3 shows the chemical composition of concentrates in an actual OBBS production plant. The feed rate is 66 t/h, the oxygen rate under standard condition is 11963 m^3/h, and the smelting temperature is 1501 K. The model is used to simulate the process with the raw material composition and process parameters.

3.3.2 Product compositions

The calculation results are shown in Table 4.

As shown in Table 4, the calculated copper matte grade is 70.67 wt.%, and the copper content in slag is 3.12 wt.%, of which relative errors are −0.14% and 0.65%, respectively, compared with the actual production results. The Sb content in copper matte and slag was 0.04 wt.% and 0.12 wt.%, respectively. Sb is mainly distributed in the slag phase, accounting for 71.07% of the total Sb in the system. The calculated results are in good agreement with the actual production results.

Table 3 Chemical composition of concentrates (wt.%)

Cu	Fe	S	Sb	SiO_2	CaO
24.35	26.76	28.37	0.10	6.35	2.40

Table 4 Comparison of composition with actual plant data for OBBS

Sample	Content/wt.%				Sb distribution/%
	Cu	Fe	S	Sb	
Industrial matte	70.77	5.52	20.22	0.04	12.48
Calculated matte	70.67	4.43	20.29	0.04	12.74
Industrial slag	3.10	42.54	0.85	0.13	71.15
Calculated slag	3.12	40.78	0.81	0.12	71.07

4 Model applications

4.1 Key indicators

4.1.1 Copper matte grade and smelting temperature

In the present work, the blowing rates of oxygen and air are adjusted to model the copper matte grade change while maintaining the oxygen-enriched concentration at 72.99 vol.%. Theoretical temperature and copper matte grade are shown in Fig. 5 and Fig. 6, respectively.

In Fig. 5, theoretical temperature increases significantly with increasing matte grade. The actual simulated temperature is 1501 K and does not vary with copper matte grade. As seen in Fig. 6, the actual matte grade is lower than theoretical data due to the mechanical entrainment of slag and copper matte during the actual production process [53].

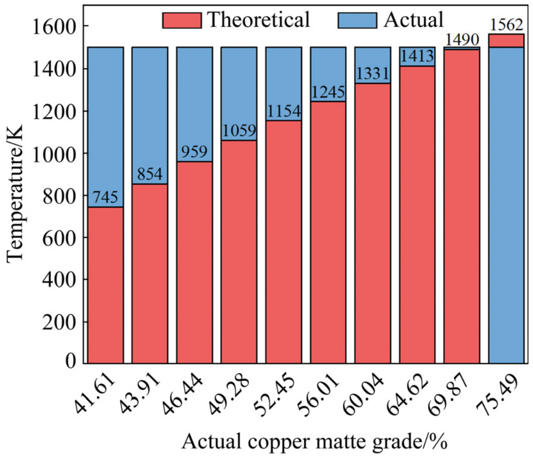

Fig. 5 Calculated and actual copper smelting temperatures versus actual copper matte grade

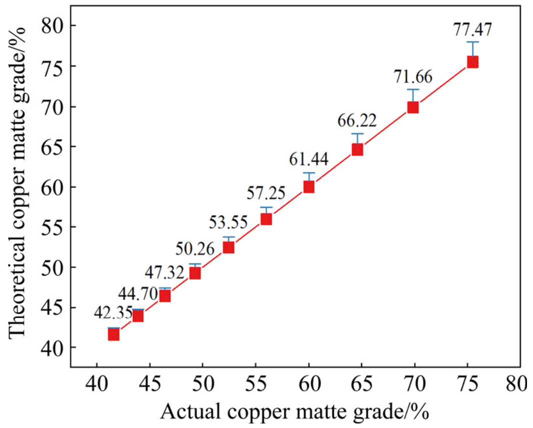

Fig. 6 Calculated copper matte grade versus actual copper matte grade

4.1.2 Oxygen and sulfur partial pressures

The partial pressures of oxygen and sulfur indicate the magnitude of oxidation and sulfidation capacity in the smelting system, which has a very important influence on the oxidation and volatilization of elements. SHISHIN et al [24] determined the lg p_{O_2} and lg p_{S_2} at T=1473 K, p_{SO_2}=(1.013−3.039)×10^4 Pa in silica saturated fayalite slag. ROGHANI et al [25] investigated the partial pressures p_{O_2} and p_{S_2} at T=1573 K and p_{SO_2}=1.013×10^4 Pa. The lg p_{O_2} and lg p_{S_2} are calculated at T=1501 K and p_{SO_2}=3.4442×10^4 Pa by using spinel-saturated slag. Under industrial production conditions T=1501 K and p_{SO_2}=(2.3299−3.5455)×10^4 Pa, the model is used to calculate lg p_{O_2} and lg p_{S_2} in the present work, as shown in Fig. 7 and Fig. 8, respectively.

At a given copper matte grade and temperature, the oxygen and sulfur partial pressures increase with an increasing SO_2 partial pressure. In this work, the lg p_{O_2} increases from −8.95 to −7.62 with an increasing matte grade from 41.6% to 75.49%, whereas the lg p_{S_2} decreases from −2.15 to −4.12. The modeling results in this work agree with published data in the literature [24,25]. The p_{SO_2}

increases from 2.3299×10^4 to 3.5455×10^4 Pa while increasing matte grade from 41.61% to 75.49% in the modeling process, resulting in a faster rise rate of oxygen partial pressure and a faster decrease rate of sulfur partial pressure than the theoretical values.

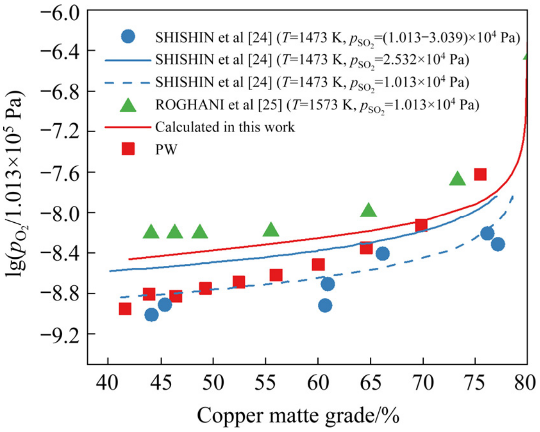

Fig. 7 Comparison of calculated oxygen partial pressures with published data

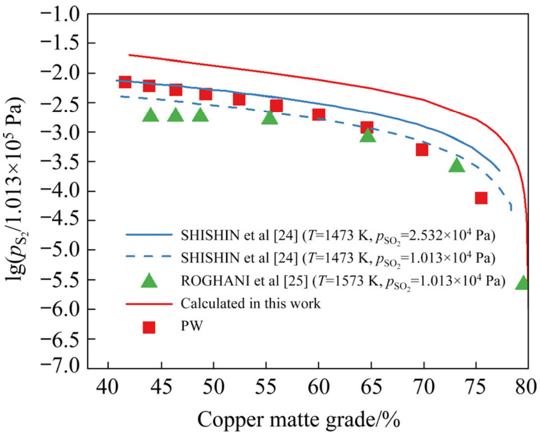

Fig. 8 Comparison of calculated sulfur partial pressures with published data

4.2 Element behavior

4.2.1 Main elements behavior

Copper and iron should be preferred to pay attention in the copper smelting process. Figure 9 shows the data for the copper content in the slag to demonstrate general trends and the effect of matte grade. Results from the literature are also plotted in the graphs for comparison.

As shown in Fig. 9(a), copper contents in slags increase with the increase of matte grade and oxygen partial pressure. TAKEDA [54] determined the Cu content in slag at 25 wt.% SiO_2 and silica saturated. CHEN et al [8] and AVARMAA et al [54] measured the Cu losses in FeO_x−SiO_2 slag. Copper losses occur as dissolved Cu in slag and as entrained matte in slag, with the latter being predominant. Oxygen enriched gas is blown from the bottom to copper matte, and high Fe/SiO_2 ratio slag is adopted in OBBS [56], in which copper is mainly entrained in the slag phase. The Cu content in the OBBS slag is significantly higher than the values reported in the literature for the copper smelting process. It is close to the values for the copper matte converting process [55].

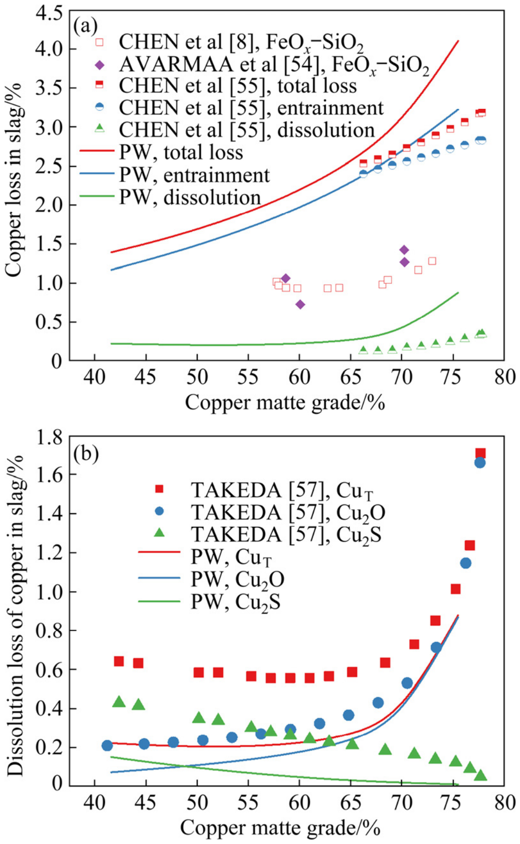

Fig. 9 Total loss (a) and dissolution loss (b) of copper in slag

The dissolved forms of copper in the slag include Cu_2S and Cu_2O, as shown in Fig. 9(b). TAKEDA [57] determined the Cu content in slag at 25 wt.% SiO_2 and silica saturated state. The increase in equilibrium p_{O_2} with matte grade (Fig. 7) should favor the oxidation of copper into the slag while reducing Cu_2S content. The data reported in the literature [57] differ somewhat from the modeling values in the present study, due to differences with experimental temperatures and crucible materials, but the trends are generally consistent.

The modeling data obtained on the solubilities of FeO and Fe_3O_4 in the iron silicate slag as a function of matte grade are illustrated in Fig. 10.

The FeO content in slag rises slowly to 29.55 wt.% and then falls to 25.84 wt.% when copper matte grade increases from 41.61% to 75.49%. At this point, the Fe_3O_4 content rises sharply from 10.88 wt.% to 27.78 wt.% with increasing matte grade. Fe content is sufficient in copper matte when the matte grade is low. Fe is oxidized to form FeO and Fe_3O_4 into the slag with increasing p_{O_2}. When the copper matte grade and p_{O_2} are further increased, but the Fe content is insufficient, the FeO content in the slag is reduced due to the generation of Fe_3O_4.

The mass of copper matte, slag phase, and gas phase versus the matte grade is plotted in Fig. 11. As the grade of copper matte increases, the mass of copper matte decreases, and the mass of slag and flue gas phase increases. Fe in copper matte is oxidized to iron oxide into slag, S in copper matte is oxidized to SO_2 and SO_3 into flue gas, respectively.

4.2.2 Antimony behavior

The mass changes of Sb-bearing compounds in copper matte, slag, and gas are presented in Fig. 12. $[Sb]_{mt}$, $\langle SbO_{1.5}\rangle_{sl}$, $(SbO)_g$ and $(SbS)_g$ denote the substances containing Sb in copper matte, slag, and flue gas, respectively. With increasing copper matte grade from 41.61% to 75.49%, $[Sb]_{mt}$ first gradually decreases to 5.89 kg and then slowly increases to 9 kg. The quality of the $\langle SbO_{1.5}\rangle_{sl}$ of the slag is significantly elevated from 30.37 to 131.58 kg. (SbS)g decreases rapidly to 2.13 kg, while $(SbO)_g$ is slightly increased in the flue gas. Figures 7 and 11 show that the mass of copper matte decreases, and the oxygen partial pressure increases with the increase of copper matte grade. $[Sb]_{mt}$ and $(SbS)_g$ are oxidized to $(SbO)_g$ and $\langle SbO_{1.5}\rangle_{sl}$. Since the modeling temperature is kept constant, the Gibbs free energy changes shown in Table 2 are not affected by the grade of copper matte. However, the activity coefficient of Sb decreases as the copper matte grade increases, so further increasing the Cu content instead increases the Sb content in the copper matte. In addition, the copper matte and slag contain small amounts of $[SbO_{1.5}]_{mt}$ and $\langle Sb\rangle_{sl}$, respectively, due to mechanical entrapment during the copper smelting process.

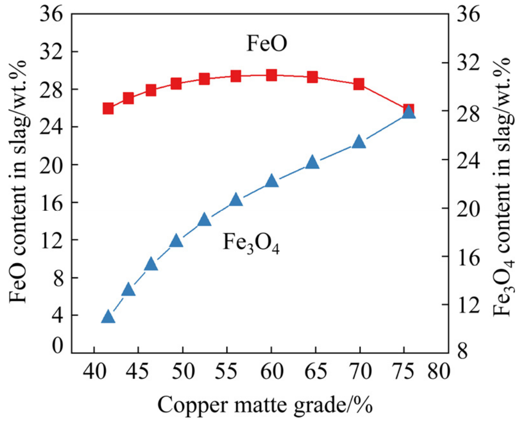

Fig. 10 Calculated contents of FeO and Fe_3O_4 in slag versus copper matte grade

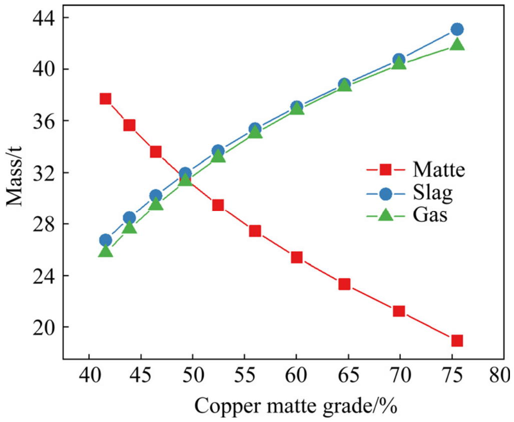

Fig. 11 Calculated mass of products versus copper matte grade

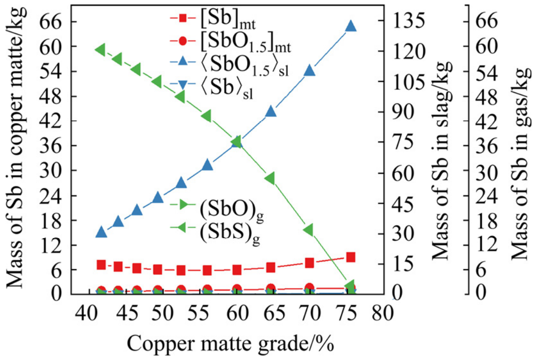

Fig. 12 Mass of Sb-bearing species in multi-phase as function of copper matte grade

The effects of copper matte grade on the contents of Sb in copper matte, slag, and flue gas are represented in Fig. 13. As copper matte grade increases from 41.61% to 75.49%, the Sb content in copper matte slowly increases from 0.020 wt.% to 0.051 wt.%, in slag it gradually increases from 0.048 wt.% to 0.13 wt.%, while in flue gas it rapidly decreases from 0.18 wt.% to 0.0042 wt.%. The decrease in the mass of copper matte strengthens the trend of increasing the Sb content in copper matte. The Sb content in slag increases slowly due to higher slag mass. The mass of gas and $(SbS)_g$ decreases simultaneously, which results in a sharp decrease in the Sb content in the gas.

The activity coefficients of Sb in matte and $SbO_{1.5}$ in the slag are plotted in Fig. 14. The activity coefficient of Sb decreases with an increasing copper matte grade, while the activity coefficient of $SbO_{1.5}$ in slag does not vary with the change of copper matte grade.

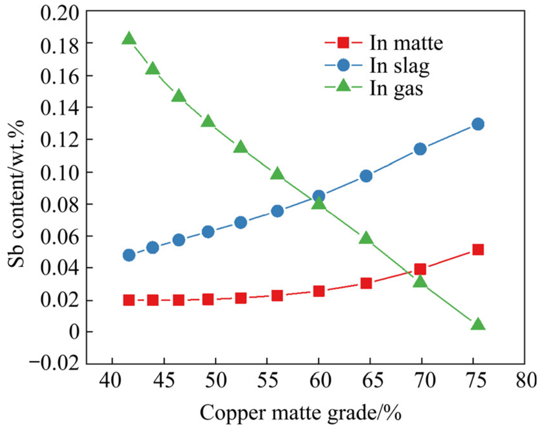

Fig. 13 Content of Sb in multi-phase as function of copper matte grade

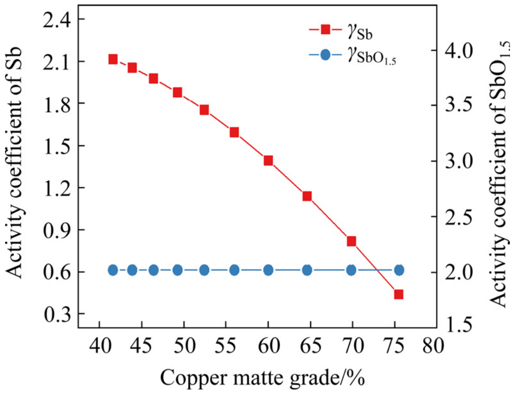

Fig. 14 Activity coefficient of Sb in copper matte and that of $SbO_{1.5}$ in iron silicate slag versus copper matte grade

The distribution ratio of element Me between slag and copper matte ($L_{Me}^{slag/matte}$) can be described by Eq. (22):

$$L_{Me}^{slag/matte} = \frac{< Me >}{[Me]} \tag{22}$$

where [Me] refers to the Me content (wt.%) in copper matte and <Me> to Me content (wt.%) in slag.

Figure 15 shows a trend of distribution ratio of Sb with the grade of copper matte. The $L_{Sb}^{slag/matte}$ is always greater than 1 in OBBS, indicating that Sb is preferentially oxidized into the slag, which is consistent with the above analysis results. The $L_{Sb}^{slag/matte}$ rises slowly to 3.30 and then decreases to 2.52 as the copper matte grade rises from 41.61% to 75.49%. The result indicates that there is an optimum grade of copper matte when only the removal of the Sb is considered.

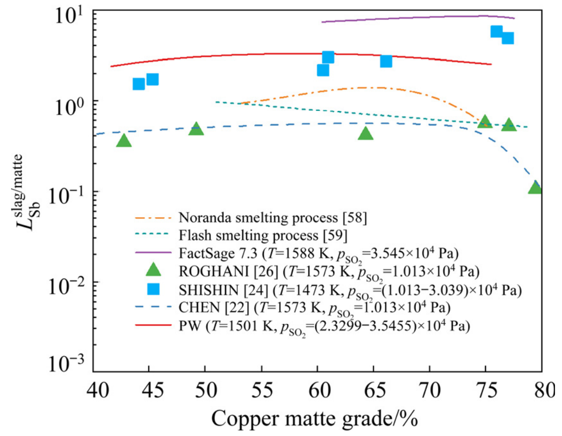

Fig. 15 Distribution ratios of Sb between iron silicate slag and copper matte versus copper matte grade

The trend of $L_{Sb}^{slag/matte}$ in Noranda smelting process [58] and ROGHANI [26], CHEN et al [22], SHISHIN et al [24] research results is in accordance with that in this work. Sb distribution coefficient is below 1 in the Noranda smelting process when high-grade copper matte is produced. Similar results are also found by ROGHANI [26] and CHEN et al [22], which means that it is difficult to remove antimony by slagging under these conditions. The $L_{Sb}^{slag/matte}$ is less than 1 and decreases as the grade of copper matte increases in the flash smelting process [59]. In this process, Sb remains in copper matte compared to slag, and the high grade of copper matte is not conducive to Sb removal.

4.3 Multi-phase distribution

4.3.1 Raw material composition

The effects of Cu, S, and Sb contents in the concentrate on the distribution of Sb in OBBS are calculated. The modeling results are shown in Fig. 16 and Fig. 17.

Figures 16(a) shows the effect of the copper content in the feed on the Sb distribution to three phases. As the Cu content in the concentrate increases from 14.35 wt.% to 26.55 wt.%, the content of other elements such as Fe and S decreases accordingly. The amount of oxygen consumed decreases. The equilibrium oxygen

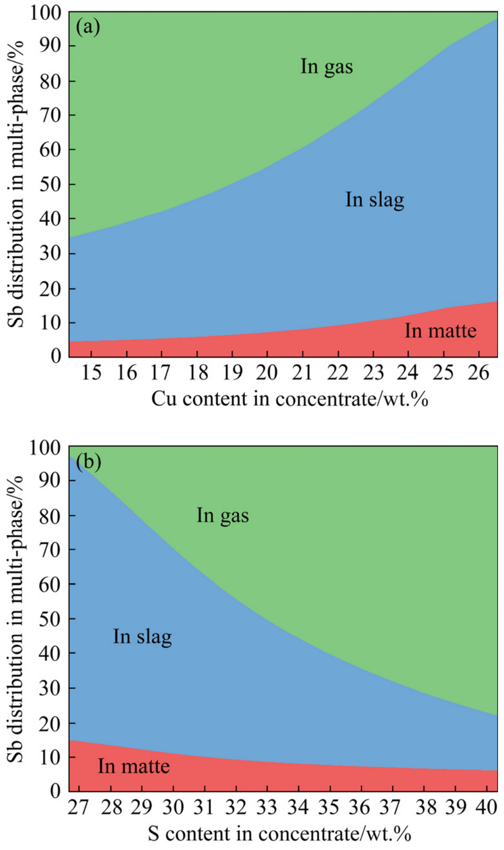

Fig. 16 Distribution of Sb in three phases as function of Cu (a) and S (b) contents in concentrate

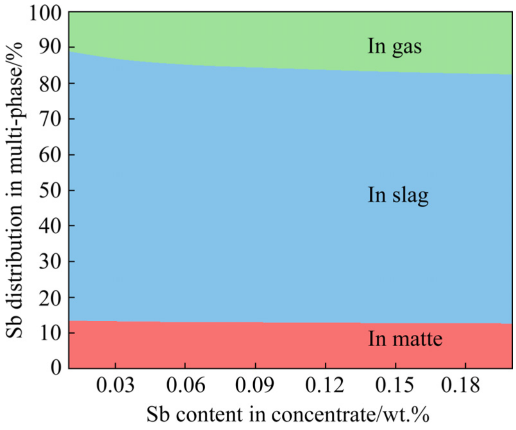

Fig. 17 Distribution of Sb in three phases as function of Sb content in concentrate

partial pressure p_{O_2} and the copper matte grade increase with a constant total oxygen supply. The Sb distribution to the slag increases with increasing Cu content because of the increase of the oxygen partial pressure in the gas, which enhances the oxidation of antimony to the slag phase. The distribution of Sb to the gas phase decreases significantly. The activity coefficient of Sb in the matte decreases with an increasing matte grade, which results in raising the Sb distribution to the copper matte phase. Thus, increasing the Cu content in the concentrate favors the enrichment of Sb into the slag, leading to a decrease in the Sb removal rate from the copper matte.

Figure 16(b) shows the calculated distribution of Sb in the three phases as a function of S content in concentrate. As the S content in the concentrate increases, varying from 26.67% to 40.37%, the system equilibrium $\lg p_{S_2}$ increases from −4.05 to −2.08, $\lg p_{O_2}$ decreases from −7.68 to −8.72, and copper matte grade decreases from 75.16% to 45.67%. More Sb removed from slag phases by the gas phase as Sb is dominantly evaporated as SbS into the gas phase. The decrease in copper matte grade results in a slight decrease in the distribution of Sb assigned to copper matte. Therefore, increasing the S content in concentrate is not conducive to the enrichment of Sb into the slag.

Figure 17 shows the relationship between the Sb content in the feed and its distribution to the matte, slag, and gas phases, respectively, for Sb contents in the feed between 0.01 wt.% and 0.20 wt.%. As Sb content in the concentrate increases, the Sb distribution in copper matte and slag decreases, and Sb is gradually enriched to the gas. Since the Sb content in the concentrate is relatively small, its content has little effect on the grade of copper matte in the system, the melting temperature, the mass of the multi-phase products, the equilibrium oxygen, and sulfur partial pressure. Sb distribution behavior is mainly determined by its activity in each phase. The activity of Sb and $SbO_{1.5}$ in matte and slag increases as the Sb content in the feed increases, which results in a low distribution in matte and slag. While increasing the Sb content in the concentrate is beneficial to reducing the proportion of Sb in the copper matte, the Sb content in the copper matte increased from 0.0042 wt.% to 0.081 wt.% when the Sb content in concentrate increases from 0.01 wt.% to 0.20 wt.%. To reduce the impurity content in copper matte, raw materials containing lower impurities should be used as much as possible, which facilitates the removal of Sb.

4.3.2 Process parameters

Figure 18 shows the effects of the process parameters such as matte grade, oxygen-enriched concentration on the distribution of Sb in the OBBS process.

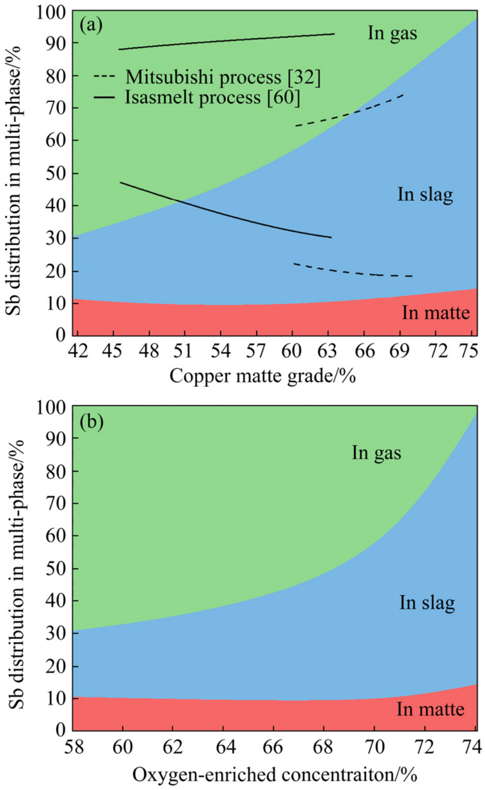

Fig. 18 Distribution of Sb in three phases as function of copper matte grade (a), and oxygen-enriched concentration (b)

In Fig. 18(a), the variations in the calculated equilibrium distribution of Sb in the gas, slag, and matte phases with matte grade at 1501 K are presented. These results show that more than 69% of antimony volatilizes to the gas phase at low matte grade of 41.61%. However, as the matte grade increases, the relative portion of Sb that volatilizes to the gas phase decreases significantly to less than 3% at a matte grade of about 76% with marked increase in the distribution to the slag phase. The Sb distribution in copper matte first gradually decreases and then slowly increases, which is consistent with the trend of mass change of Sb-containing compounds in matte. As discussed in the previous section, the p_{O_2} increases and p_{S_2} decreases with an increasing matte grade, thus causing lower volatilization of Sb as SbS. The matte mass and the activity coefficient of Sb in the matte are decreased, which result in a high Sb distribution in copper matte at both high and low matte grades [25]. The trend of Sb distribution with the copper matte grade for the Mitsubishi smelting [32] and Isa smelting processes [60] are consistent with the results in this work. However, there are differences in the values due to different process parameters used.

The Sb distribution in three phases as a function of oxygen-enriched concentration is illustrated in Fig. 18(b), which is consistent with trends influenced by copper matte grade. The lg p_{O_2} increases from −8.95 to −7.59 with increasing the oxygen-enriched concentration from 58.00% to 74.10%. A large amount of SbS in the flue gas is oxidized into the slag. With the increase in copper matte grade from 43.41% to 75.57% and the decrease in matte mass from 36.09 to 18.90 t, the Sb activity in copper matte first slowly increases and then rapidly decreases. The distribution of Sb in matte first decreases and then increases. Increasing the oxygen-enriched concentration facilitates the targeted enrichment of Sb into the slag.

Figure 19 shows that the effects of process parameters such as oxygen/ore ratio and smelting temperature on the distribution of Sb in the OBBS process.

The effect of the oxygen/ore ratio on the Sb distribution ratio is shown in Fig. 19(a). The multi-phase distribution proportion of Sb in flue gas, slag, and copper matte is 27.59%−10.64%, 60.62%−75.80%, and 11.79%−13.56%, respectively, as the oxygen/ore ratio increases from 139.20 to 173.9 m^3/t. The system equilibrium oxygen partial pressure increased lg p_{O_2} from −8.53 to −7.60, and (SbS)$_g$ in the flue gas is reduced due to oxidation into the slag. The copper matte grade increases from 59.33% to 75.63%, and the Sb activity coefficient in copper matte decreases from 1.43 to 0.43. The percentage of Sb distributed to copper matte increases. The proportion of Sb in copper matte does not out-perform the trough, compared to that affected by copper matte grade and oxygen-enriched concentration variations. Because of the small range of variation in the oxygen/ore ratio, the minimum value of Sb distribution in copper matte occurs when the oxygen/ore ratio is less than 139.20 m^3/t. Therefore, increasing the oxygen/ore ratio and appropriately sacrificing the quality of copper matte facilitate the targeted enrichment of Sb in slag.

The effect of smelting temperature on the Sb distribution is shown in Fig. 19(b). The percentage of Sb distribution in copper matte and flue gas increases to 16.28% and 28.67%, respectively, and decreases from 81.88% to 55.04% in slag as temperature increases from 1423 to 1603 K. According to Table 2, the increase in temperature discourages the generation of $SbO_{1.5}$ in slag. At the same time, the copper matte grade slightly increases, and the vapor pressures of SbS and SbO in the gas increase [30]. As a result, the removal of Sb as gaseous SbS and SbO species increases with an increasing temperature. The behavior of the Sb in the gas and slag agrees well with a previous study [32], but the distribution in the copper matte is opposite with increasing temperature.

4.4 Process parameters optimization

The copper matte grade, smelting temperature, and product mass are important indicators for evaluating the production process. These indicators are influenced by the raw material composition and process parameters, which in turn affect the Gibbs free energy change and activity coefficient of compounds in multi-phase. The effects of concentrate composition and process parameters on the multi-phase partitioning behavior of Sb are systematically investigated in the previous section. The three indicators have been changed due to various factors. A certain indication should be fixed before comparing the multi-phase allocation behavior of elements between different processes.

The industrial production data for three OBBS production lines are collected in Tables 5 and 6.

In Table 6, the slag rate L_{slag} and gas rate L_{gas} are calculated by the followed Eqs. (23) and (24), respectively:

$$L_{\text{slag}}=\frac{m_{\text{slag}}}{m_{\text{matte}}} \tag{23}$$

$$L_{\text{gas}}=\frac{m_{\text{gas}}}{m_{\text{matte}}} \tag{24}$$

where m_{slag}, m_{gas} and m_{matte} are masses of slag, gas and copper matte, respectively.

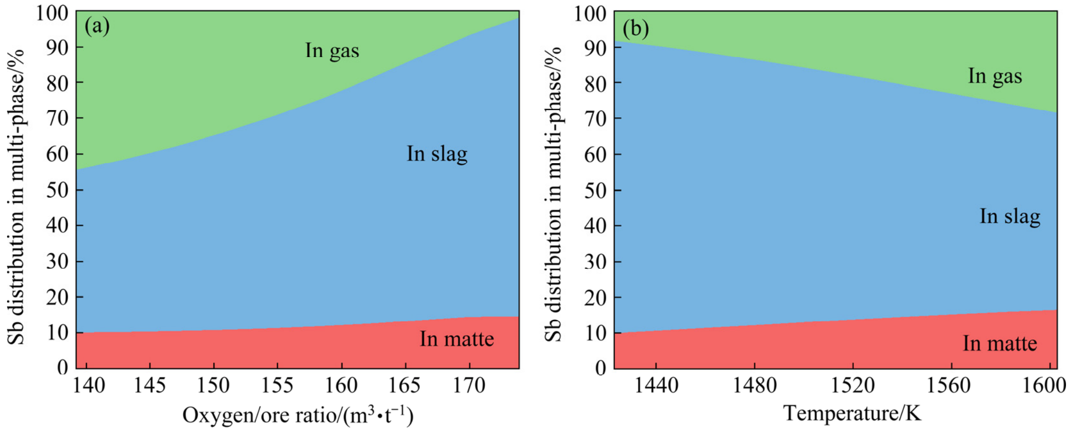

Fig. 19 Distribution of Sb in three phases as function of oxygen/ore ratio (a) and smelting temperature (b)

Table 5 Chemical compositions of concentrate and product in different production lines

Production line	Phase	Chemical composition/wt.%				Distribution of Sb/%
		Cu	Fe	S	Sb	
OBBS-I	Concentrate	22.67	24.89	25.61	0.10	100
	Matte	70.68	3.44	19.69	0.04	11.50
	Slag	2.63	40.88	0.60	0.14	82.90
OBBS-II	Concentrate	24.35	26.76	28.37	0.10	100
	Matte	70.77	5.52	20.22	0.04	12.48
	Slag	3.10	42.54	0.85	0.13	71.15
OBBS-III	Concentrate	25.06	24.44	28.22	0.047	100
	Matte	70.29	4.84	20.14	0.04	26.77
	Slag	3.37	43.38	0.81	0.03	35.95

Table 6 Process parameters in different production lines

Parameter	OBBS-I	OBBS-II	OBBS-III
Matte grade/%	70.68	70.77	70.29
Oxygen-enriched concentration/%	73.47	72.99	80.45
Ratio of oxygen to ore/($m^3 \cdot t^{-1}$)	156.20	164.23	161
Bath temperature/K	1469	1501	1541
Slag rate	2.00	1.96	1.61
Gas rate	1.81	1.94	1.54

As shown in Tables 5 and 6, to produce the same grade of copper matte, the process parameters (oxygen/ore ratio, oxygen-enriched concentration) vary with the composition (Cu, Fe, S, and Sb) of the raw material. At this point, the partitioning behavior of Sb in the various processes is also different and plotted in Fig. 20. The essential indicators corresponding to each process are shown in Fig. 21.

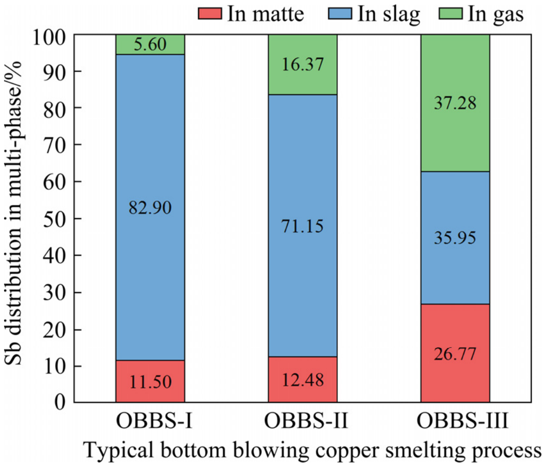

Fig. 20 Distribution of Sb in typical OBBS processes

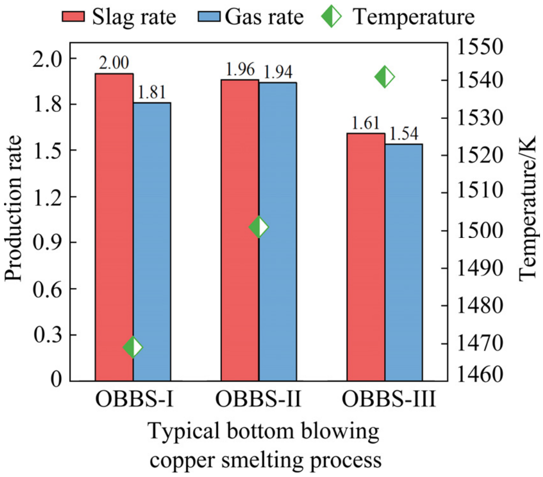

Fig. 21 Key indicators in typical OBBS processes

The Sb removal rate in OBBS-I and OBBS-II is approximately 90%, but the Sb in the former process is more enriched in the slag, accounting for about 83%. The distribution of Sb in three phases in OBBS-III does not differ significantly, and the Sb removal rate is lowest in three production lines. This is mainly because lower operating temperature and greater slag rate are used in OBBS-I, as shown in Fig. 21. As previously analyzed, slightly lower melting temperature and more slag mass are advantageous for Sb to be separated from the slag phase. More Sb is removed from the copper matte and slag phases by the gas phase with increasing temperature [60].

5 Conclusions

(1) The reaction mechanism of the associated element Sb in the oxygen-enriched copper smelting process was revealed. Reinforcing the reaction in the flue gas phase reduces the volatilization of Sb in flue gas and increases it into the melting bath. Sb_2O_3 in the slag can be reduced by sulfide and reducing agent to SbS, SbO volatilization into gas, or Sb into the copper matte. In the absence of sufficient oxygen, Sb is difficult to be removed from the copper matte by oxidation.

(2) The distribution trends of Sb in four typical copper smelting processes were analyzed. Sb is easier to volatilize into flue gas in bath smelting than in the flash smelting process. Blowing oxygen-enriched air to melt bath, Sb in the copper matte is fully oxidized into the slag. In the top-blowing and side-blowing melting processes, Sb in the slag is re-volatilized into the flue gas with reductant and low oxygen-enriched concentration air.

(3) A multi-phase equilibrium thermodynamic model for copper oxygen-enriched bottom-blowing was developed. The copper matte and slag compositions were calculated under industrial production conditions. The calculated results agreed well with the actual production results, which proved the accuracy of the model. The model was also used to calculate the trends of copper loss in slag, oxygen partial pressure, and sulfur partial pressure in gas. The calculation results were basically consistent with the literature, which proved the reliability of the model.

(4) The raw material composition and process parameters were optimized. With the increase

of Cu content in concentrate, oxygen-enriched concentration and oxygen/ore ratio, more Sb in the flue gas was oxidized into the slag. As the sulfur content increased, Sb is mainly volatilized into the flue gas. Sb was concentrate has little effect on its own distribution. As the melting temperature increased, antimony in slag was distributed to the flue gas and copper matte. The simulation results were in good agreement with the production results, demonstrating that the model can guide the clean treatment of complex antimony-bearing resources in the oxygen-enriched smelting process.

Acknowledgments

The authors are grateful for the financial supports from the National Natural Science Foundation of China (Nos. 51904351, 51620105013, U20A20273), the National Key R&D Program of China (Nos. 2018YFC1900306, 2019YFC1907400), the Major Science and Technology Innovation Project of Shandong Province, China (No. 2019JZZY010404), and the Innovation Driven Project of Central South University, China (No. 2020CX028).

References

[1] FLORES G A, RISOPATRON C, PEASE J. Processing of complex materials in the copper industry: Challenges and opportunities ahead [J]. JOM, 2020, 72(10): 3447−3461.

[2] HOLGERSSON S, STEENARI B M, BJÖRKMAN M, CULLBRAND K. Analysis of the metal content of small-size waste electric and electronic equipment (WEEE) printed circuit boards—Part 1: Internet routers, mobile phones and smartphones [J]. Resources, Conservation and Recycling, 2018, 133: 300−308.

[3] BAGHERIFAM S, BROWN T C, FELLOWS C M, NAIDU R. Bioavailability of arsenic and antimony in terrestrial ecosystems: A review [J]. Pedosphere, 2019, 29(6): 681−720.

[4] TABELIN C B, PARK I, PHENGSAART T, JEON S, VILLACORTE-TABELIN M, ALONZO D, YOO K, ITO M, HIROYOSHI N. Copper and critical metals production from porphyry ores and E-wastes: A review of resource availability, processing/recycling challenges, socio-environmental aspects, and sustainability issues [J]. Resources, Conservation and Recycling, 2021, 170: 105610.

[5] MA E. Electronic waste management and treatment technology [M]. Amsterdam: Elsevier, 2019: 247–267.

[6] WOOD J, CREEDY S, MATUSEWICZ R, REUTER M. Secondary copper processing using Outotec Ausmelt TSL technology [C]//Proceedings of MetPlant 2011. Carlton South: The Australasian Institute of Mining & Metallurgy, 2011: 460−467.

[7] SINEVA S, SHEVCHENKO M, SHISHIN D, HIDAYAT T, CHEN J, HAYES P C, JAK E. Phase equilibria and minor element distributions in complex copper/slag/matte systems [J]. JOM, 2020, 72(10): 3401−3409.

[8] CHEN M, AVARMAA K, KLEMETTINEN L, O'BRIEN H, SUKHOMLINOV D, SHI J J, TASKINEN P, JOKILAAKSO A. Recovery of precious metals (Au, Ag, Pt, and Pd) from urban mining through copper smelting [J]. Metallurgical and Materials Transactions B, 2020, 51: 1495−1508.

[9] HELLSTÉN N, KLEMETTINEN L, SUKHOMLINOV D, O BRIEN H, TASKINEN P, JOKILAAKSO A, SALMINEN J. Slag cleaning equilibria in iron silicate slag−copper systems [J]. Journal of Sustainable Metallurgy, 2019, 5(4): 463−473.

[10] KLAFFENBACH E, MOSTAGHEL S, GUO M X, BLANPAIN B. Thermodynamic analysis of copper smelting, considering the impact of minor elements behavior on slag application options and Cu recovery [J]. Journal of Sustainable Metallurgy, 2021, 7(2): 664−683.

[11] GHODRAT M, SAMALI B, RHAMDHANI M, BROOKS G. Thermodynamic-based energy analysis of precious metal recovery out of waste printed circuit board through black copper smelting process [J]. Energies, 2019, 12(7): 1313.

[12] GU Kun-hong, LIU Wei, HAN Jun-wei, OU Zhen-yu, WU Di-xiu, QIN Wen-qing. Arsenic and antimony extraction from high arsenic smelter ash with alkaline pressure oxidative leaching followed by Na_2S leaching [J]. Separation and Purification Technology, 2019, 222: 53−59.

[13] XUE Jian-rong, LONG Dong-ping, ZHONG Hong, WANG Shuai, LIU Li-hua. Comprehensive recovery of arsenic and antimony from arsenic-rich copper smelter dust [J]. Journal of Hazardous Materials, 2021, 413: 125365.

[14] TAN Cheng, LI Lei, ZHONG Da-peng, WANG Hua, LI Kong-zhai. Separation of arsenic and antimony from dust with high content of arsenic by a selective sulfidation roasting process using sulfur [J]. Transactions of Nonferrous Metals Society of China, 2018, 28(5): 1027−1035.

[15] ZHONG Da-peng, LI Lei. Separation of arsenic from arsenic−antimony-bearing dust through selective oxidation−sulfidation roasting with CuS [J]. Transactions of Nonferrous Metals Society of China, 2020, 30(1): 223−235.

[16] YAO Wen-ming, MIN Xiao-bo, LI Qing-zhu, LI Kai-zhong, WANG Yun-yan, WANG Qing-wei, LIU Hui, QU Sheng-li, DONG Zhun-qin, QU Chao, CHEN Tao, SONG Chao. Formation of arsenic−copper-containing particles and their sulfation decomposition mechanism in copper smelting flue gas [J]. Transactions of Nonferrous Metals Society of China, 2021, 31(7): 2153−2164.

[17] WANG Qin-meng, WANG Qiong-qiong, TIAN Qing-hua, GUO Xue-yi. Simulation study and industrial application of enhanced arsenic removal by regulating the proportion of concentrates in the SKS copper smelting process [J]. Processes, 2020, 8(4): 385.

[18] HINO M, TOGURI J M. Antimony activities in copper mattes [J]. Metallurgical Transactions B, 1987, 18(1): 189−194.

[19] MENDOZA D, HINO M, ITAGAKI K. Phase relations and activity of antimony in Cu−Fe−S−Sb system at 1473 K [J]. Materials Transactions, 2002, 43(5): 1166−1172.

[20] LYNCH D C, AKAGI S, DAVENPORT W G. Thermochemical nature of minor elements in copper

smelting mattes [J]. Metallurgical & Materials Transactions B, 1991, 22(5): 677−688.

[21] NAGAMORI and M. Thermodynamic behaviour of arsenic and antimony in copper matte smelting — A novel mathematical synthesis [J]. Canadian Metallurgical Quarterly, 2001, 40(4): 499−522.

[22] CHEN Chun-lin, ZHANG Ling, WRIGHT S, JAHANSHAHI S. Thermodynamic modelling of minor elements in copper smelting processes [C]//Sohn International Symposium on Advanced Processing of Metals & Materials: Principles. San Diego, 2006: 335−348.

[23] SHUVA M A H, REUTER M A, BROOKS G A, MASOOD S. Thermodynamics data of valuable elements relevant to e-waste processing through primary and secondary copper production: A review [J]. Journal of Cleaner Production, 2016, 131: 795−809.

[24] SHISHIN D, HIDAYAT T, CHEN J, HAYES P C, JAK E. Combined experimental and thermodynamic modelling investigation of the distribution of antimony and tin between phases in the Cu−Fe−O−S−Si system [J]. Calphad, 2019, 65: 16−24.

[25] ROGHANI G, TAKEDA Y, ITAGAKI K. Phase equilibrium and minor element distribution between FeO_x−SiO_2−MgO-based slag and Cu_2S−FeS matte at 1573 K under high partial pressures of SO_2 [J]. Metallurgical and Materials Transactions B, 2000, 31(4): 705−712.

[26] ROGHANI G. Phase equilibrium and minor elements distribution between slag and copper matte under high partial pressures of SO_2 [C]//International Conference on Molten Slags Fluxes & Salts. Sydney, 1997: 693−703.

[27] MITEVSKA N, ŽIVKOVIĆ Ž D. Thermodynamics of As, Sb and Bi distribution during reverb furnace smelting [J]. Journal of Mining and Metallurgy (Section B): Metallurgy, 2002, 38(1/2): 93−102.

[28] PADILLA R, RUIZ M C. Behavior of arsenic, antimony and bismuth at roasting temperatures [C]//Drying, Roasting, and Calcining of Minerals. Cham: Springer, 2015: 43−50.

[29] TASKINEN P, SEPP L K, LAULUMAA J, POIJÄRVI J. Oxygen pressure in the Outokumpu flash smelting furnace—Part 1: Copper flash smelting settler [J]. Mineral Processing and Extractive Metallurgy, 2001, 110(2): 94−100.

[30] CHAUBAL P C, SOHN H Y, GEORGE D B, BAILEY L K. Mathematical modeling of minor-element behavior in flash smelting of copper concentrates and flash converting of copper mattes [J]. Metallurgical Transactions B, 1989, 20(1): 39−51.

[31] FONT J M, REDDY R G. Modelling of antimonate capacity in copper and nickel smelting slags [J]. Mineral Processing and Extractive Metallurgy, 2005, 114(3): 160−164.

[32] SURAPUNT S. Computer simulation of the distribution behavior of minor elements in the copper smelting process [J]. Science & Technology Asia, 2004, 9(4): 61−68.

[33] LUO Hong-lin, LIU Wei, QIN Wen-qing, ZHENG Yong-xing, YANG Kang. Cleaning of high antimony smelting slag from an oxygen-enriched bottom-blown by direct reduction [J]. Rare Metals, 2019, 38(8): 800−804.

[34] HAGA K, ALTANSUKH B, SHIBAYAMA A. Volatilization of arsenic and antimony from tennantite/tetrahedrite ore by a roasting process [J]. Materials Transactions, 2018, 59(8): 1396−1403.

[35] ŽIVKOVIĆ Ž, ŠTRBAC N, GRUJIČIĆ D, BOYANOV B. Kinetics and mechanism of Sb_2S_3 oxidation process [J]. Thermochimica Acta, 2002, 383(1/2): 137−143.

[36] PADILLA R, ARACENA A, RUIZ M C. Reaction mechanism and kinetics of enargite oxidation at roasting temperatures [J]. Metallurgical and Materials Transactions B, 2012, 43(5): 1119−1126.

[37] LUO Yin-hua. Practice of technological transformation of Fubang oxygen-enriched side-blown smelting furnace [J]. China Nonferrous Metallurgy, 2014, 43(2): 51−53. (in Chinese)

[38] KAPUSTA J. Sonic injection in sulphide bath smelting: An update [J]. Journal of the Southern African Institute of Mining and Metallurgy, 2018, 118(11): 1131−1139.

[39] WOOD J, HUGHES S. Future development opportunities for the Outotec Ausmelt process [C]//Proceedings of Copper 2016. Kobe, 2016: 361−372.

[40] HOGG B, NIKOLIC S, VOIGT P, TELFORD P. ISASMELT^{TM} technology for sulfide smelting [C]//Extraction 2018. Cham: Springer, 2018: 149−158.

[41] SCHLESINGER M E, SOLE K C, DAVENPORT W G. Extractive metallurgy of copper [M]. Amsterdam: Elsevier, 2011.

[42] CHENG Li-zhen, XU Xin. Research progress on distribution of impurity elements in copper matte smelting and its synthetic recycling [J]. Nonferrous Materials and Engineering, 2016, 37(3): 103−109. (in Chinese)

[43] ALVEAR G R, HUNT S P, ZHANG B. Copper ISASMELT - Dealing with impurities [C]//Sohn International Symposium on Advanced Processing of Metals and Materials. San Diego, 2006: 673−685.

[44] WAN Xing-bang, TASKINEN P, SHI Jun-jie, KLEMETTINEN L, JOKILAAKSO A. Reaction mechanisms of waste printed circuit board recycling in copper smelting: The impurity elements [J]. Minerals Engineering, 2021, 160: 106709.

[45] NÉRON A, LANTAGNE G, MARCOS B. Computation of complex and constrained equilibria by minimization of the Gibbs free energy [J]. Chemical Engineering Science, 2012, 82: 260−271.

[46] ACUÑA C, YAZAWA A. Behaviours of arsenic, antimony and lead in phase equilibria among copper, matte and calcium or barium ferrite slag [J]. Transactions of the Japan Institute of Metals, 1987, 28(6): 498−506.

[47] YAZAWA A, NAKAZAWA S, TAKEDA Y. Distribution behavior of various elements in copper smelting systems [J]. JOM, 1984, 36(8): 79.

[48] TAKEDA Y, ISHIWATA S, YAZAWA A. Distribution equilibria of minor elements between liquid copper and calcium ferrite slag [J]. Transactions of the Japan Institute of Metals, 1983, 24(7): 518−528.

[49] YAZAWA A, TAKEDA Y. Equilibrium relations between liquid copper and calcium ferrite slag [J]. Transactions of the Japan Institute of Metals, 1982, 23(6): 328−333.

[50] YAZAWA A. Thermodynamic considerations of copper smelting [J]. Canadian Metallurgical Quarterly, 1974, 13(3): 443−453.

[51] NAGAMORI M, CHAUBAL P C. Thermodynamics of

copper matte converting: Part III. Steady-state volatilization of Au, Ag, Pb, Zn, Ni, Se, Te, Bi, Sb, and As from slag, matte, and metallic copper [J]. Metallurgical Transactions B, 1982, 13(3): 319−329.

[52] KAUR R R, SWINBOURNE D R, NEXHIP C. Nickel, lead and antimony distributions between ferrous calcium silicate slag and copper at 1300 °C [J]. Mineral Processing and Extractive Metallurgy, 2009, 118(2): 65−72.

[53] BELLEMANS I, WILDE E D, MOELANS N, VERBEKEN K. Metal losses in pyrometallurgical operations—A review [J]. Advances in Colloid and Interface Science, 2017, 255: 47−63.

[54] AVARMAA K, JOHTO H, TASKINEN P. Distribution of precious metals (Ag, Au, Pd, Pt, and Rh) between copper matte and iron silicate slag [J]. Metallurgical & Materials Transactions B, 2016, 47(1): 244−255.

[55] CHEN Chun-lin, ZHANG Jia-yun, BAI Meng, WEI Shou-kun. Investigation on the copper content of matte smelting slag in Peirce−Smith converter [J]. Journal of University of Science and Technology Beijing Mineral Metallurgy Material, 2001, 8(3): 177−181.

[56] WANG Qin-meng, GUO Xue-yi, TIAN Qing-hua. Copper smelting mechanism in oxygen bottom-blown furnace [J]. Transactions of Nonferrous Metals Society of China, 2017, 27(4): 946−953.

[57] TAKEDA Y. Copper solubility in matte smelting slag [C]//Molten Slags, Fluxes and Salts' 97 Conference. Sydney, 1997: 5−8.

[58] PERSSON H, IWANIC M, EL-BARNACHAWY S, MACKEY P J. The Noranda process and different matte grades [J]. JOM, 1986, 38(9): 34−37.

[59] MÄKINEN J K, JÅFS G A. Production of matte, white metal, and blister copper by flash furnace [J]. JOM, 1982, 34(6): 54−59.

[60] NAGAMORI M, ERRINGTON W J, MACKEY P J, POGGI D. Thermodynamic simulation model of the Isasmelt process for copper matte [J]. Metallurgical and Materials Transactions B, 1994, 25(6): 839−853.

铜复杂资源熔炼过程中杂质锑脱除的热力学模拟

王松松[1,2]，王亲猛[1,2]，郭学益[1,2]，田庆华[1,2]，曲胜利[3]，王 智[4]，黄明星[1,2]

1. 中南大学 冶金与环境学院，长沙 410083；
2. 有色金属资源循环利用国家地方联合工程研究中心，长沙 410083；
3. 山东恒邦冶炼股份有限公司，烟台 264109；
4. 东营方圆有色金属有限公司，东营 257091

摘　要：研究铜冶炼过程 Sb 的反应机理，分析 Sb 在 4 种典型铜冶炼工艺中多相分配差异。建立富氧底吹铜冶炼工艺的多相平衡模型，研究原料中 Cu、S 和 Sb 含量对 Sb 多相分配比的影响。同时，应用该模型研究铜锍品位、富氧浓度、熔炼温度和氧矿比(标准状态下氧气流量与精矿加料速率之比)等工艺参数对 Sb 分配行为的影响。结果表明，计算数据与实际生产结果和文献数据吻合良好。提高精矿中 Cu 含量、降低 S 和 Sb 含量，提高铜锍品位、富氧浓度和氧矿比，同时适当降低冶炼温度，有利于 Sb 向炉渣中定向富集。模拟结果可为复杂资源清洁高效处理及伴生元素综合回收提供理论指导。

关键词：铜；富氧熔炼；锑；反应机理；分配行为

(Edited by Wei-ping CHEN)